

Potential of mean force between hydrophobic solutes in the Jagla model of water and implications for cold denaturation of proteins

Moumita Maiti, Saul Weiner, Sergey V. Buldyrev, H. Eugene Stanley, and Srikanth Sastry

Citation: *J. Chem. Phys.* **136**, 044512 (2012); doi: 10.1063/1.3677187

View online: <http://dx.doi.org/10.1063/1.3677187>

View Table of Contents: <http://jcp.aip.org/resource/1/JCPSA6/v136/i4>

Published by the [American Institute of Physics](#).

Related Articles

Size and shape effects on receptor-mediated endocytosis of nanoparticles

J. Appl. Phys. **111**, 024702 (2012)

Hybrid modeling and simulation of stochastic effects on progression through the eukaryotic cell cycle

J. Chem. Phys. **136**, 034105 (2012)

Amino acid analogues bind to carbon nanotube via π - π interactions: Comparison of molecular mechanical and quantum mechanical calculations

JCP: BioChem. Phys. **6**, 01B607 (2012)

On binding of DNA-bending proteins to DNA minicircles

JCP: BioChem. Phys. **6**, 01B606 (2012)

On binding of DNA-bending proteins to DNA minicircles

J. Chem. Phys. **136**, 025102 (2012)

Additional information on *J. Chem. Phys.*

Journal Homepage: <http://jcp.aip.org/>

Journal Information: http://jcp.aip.org/about/about_the_journal

Top downloads: http://jcp.aip.org/features/most_downloaded

Information for Authors: <http://jcp.aip.org/authors>

ADVERTISEMENT

AIPAdvances

Submit Now

Explore AIP's new
open-access journal

- Article-level metrics now available
- Join the conversation! Rate & comment on articles

Potential of mean force between hydrophobic solutes in the Jagla model of water and implications for cold denaturation of proteins

Moumita Maiti,¹ Saul Weiner,² Sergey V. Buldyrev,² H. Eugene Stanley,³
and Srikanth Sastry^{1,a)}

¹Theoretical Sciences Unit, Jawaharlal Nehru Centre for Advanced Scientific Research, Jakkur Campus, Bangalore 560 064, India

²Department of Physics, Yeshiva University, 500 West 185th Street, New York, New York 10033, USA

³Center for Polymer Studies and Department of Physics, Boston University, Boston, Massachusetts 02215, USA

(Received 20 September 2011; accepted 24 December 2011; published online 25 January 2012)

Using the Jagla model potential we calculate the potential of mean force (PMF) between hard sphere solutes immersed in a liquid displaying water-like properties. Consistent estimates of the PMF are obtained by (a) umbrella sampling, (b) calculating the work done by the mean force acting on the hard spheres as a function of their separation, and (c) determining the position dependent chemical potential after calculating the void space in the liquid. We calculate the PMF for an isobar along which cold denaturation of a model protein has previously been reported. We find that the PMF at contact varies non-monotonically, which is consistent with the observed cold denaturation. The Henry constant also varies non-monotonically with temperature. We find, on the other hand, that a second (solvent separated) minimum of the PMF becomes deeper as temperature decreases. We calculate the solvent-solvent pair correlation functions for solvents near the solute and in the bulk, and show that, as temperature decreases, the two pair correlation functions become indistinguishable, suggesting that the perturbation of solvent structure by the solute diminishes as temperature decreases. The solvent-solute pair correlation function at contact grows as the temperature decreases. We calculate the cavity correlation function and show the development of a solvent-separated peak upon decrease of temperature. These observations together suggest that cold denaturation occurs when the solvent penetrates between hydrophobic solutes in configurations with favorable free energy. Our results thus suggest that cold denatured proteins are structured and that cold denaturation arises from strong solvent-solute interactions, rather than from entropic considerations as in heat denaturation. © 2012 American Institute of Physics. [doi:10.1063/1.3677187]

I. INTRODUCTION

Folding and unfolding transitions in proteins have been studied experimentally for many decades and in recent years have received considerable theoretical attention.^{1,2} Among the more unusual phenomena observed is the unfolding of some proteins when temperature is reduced from conditions where the protein is in its native state. Such “cold denaturation” has been observed experimentally^{3–5} for many different proteins in the last two decades. Similar denaturation is also observed upon increasing the pressure,^{6–10} a phenomenon first described by Kauzmann.¹¹ Although they have been the subject of many recent theoretical investigations, the cold denaturation and pressure denaturation transitions are less well understood than the protein unfolding that occurs upon increasing temperature.

Water as the solvent is believed to play a significant role in the collapse of proteins to the folded state in the normal (high temperature to low temperatures) folding process, due to the effective attraction between hydrophobic amino acids, a phenomenon understood through the theory of hydrophobic hydration.^{12,13} The solubility of the hydrophobic (H)

molecules in water has also been studied computationally^{14–18} by many investigators. The nature of hydrophobic hydration and its role in cold denaturation is less well understood, but it has recently been addressed^{19–24} using simplified models displaying properties analogous to water, e.g., anomalous thermodynamics.^{25–28} Here we follow the approach employed in Refs. 20 and 21 by using a spherically symmetric interaction potential for the solvent, i.e., the Jagla model.^{29,30}

Classical Flory theory^{31–33} relates the behavior of polymers to the second virial coefficient of the effective monomer-monomer interactions. If the second virial coefficient is negative, the polymer collapses into a globular state. If the second virial coefficient is positive, the polymer swells into a random coil conformation. It is thus useful to calculate the effective interactions between monomers in order to understand the folding behavior of polymers. The effective interaction between monomers arises as a combination of their bare interactions and those induced by the properties of the solvent. It was previously observed^{20,21} in simulations of a model hard sphere homopolymer immersed in the Jagla solvent that such a polymer goes from an unfolded state at high temperatures, to a collapsed state at intermediate temperatures, and to a second unfolded state at lower temperatures, which may be associated with cold denaturation. Based on these observations we expect that, for hard sphere solutes in the Jagla solvent, the

^{a)} Author to whom correspondence should be addressed. Electronic mail: sastry@jncasr.ac.in.

effective solute-solute interaction increases upon cooling (from temperatures where the hard-sphere polymer is collapsed) and becomes positive at low temperatures. In the present work, we study the effective solute-solute interactions in the Jagla solvent, in order to obtain insights into cold denaturation of proteins. We note, however, that the model system studied here is a minimal model for the phenomenon of interest, and it would be desirable to verify the key conclusions with more realistic models of water and proteins.

The effective interaction between solutes can be quantified by the PMF, which will be defined in detail in Sec. II. Using three different methods, we calculate the PMF between two hard sphere solutes immersed in the Jagla solvent over a range of temperatures spanning the unfolded, folded, and cold denatured states of the model polymer. Our results provide a quantitative confirmation of the observations in Refs. 20 and 21, namely, that a folding regime is present at intermediate temperatures, bracketed by cold and heat denaturation, for hard sphere polymers immersed in a Jagla solvent. We further analyze the structural change of the solvent near the solute, as well as the void space statistics in the solvent. Our results suggest that cold denaturation occurs because the solvent penetrates between hydrophobic solutes in configurations with favorable free energy, and these results thus provide insight into the mechanism of cold denaturation.

The remainder of this paper is organized as follows: In Sec. II we provide a detailed description of the interaction potential we are using and the concepts and methods we employ when we calculate the PMF and analyze void space. In Sec. III we summarize our results. In Sec. IV we discuss our results and offer our conclusions.

II. METHODS

The interaction potential $U(r)$ of Jagla solvent particles with an attractive tail is characterized by (i) the hard core diameter a , (ii) the soft core diameter b , (iii) the range of attractive interactions c , (iv) the depth of the attractive ramp U_A , and (v) the height of the repulsive ramp U_R (Fig. 1).^{30,34} These five parameters can be collapsed into three independent dimensionless ratios: b/a , c/a , and U_R/U_A . The ratio of the soft core and hard core diameters, b/a , is a sensitive control parameter that, for the purely repulsive case ($U_A = 0$), determines the fluid's hard-sphere ($b/a \sim 1$) or water-like ($b/a \sim 7/4$) behavior.³⁵ The latter value of b/a corresponds closely to the ratio of radial distances from a central water molecule to its second-neighbor and first-neighbor shells, as measured by the second-nearest-neighbor and nearest-neighbor peaks of the oxygen-oxygen radial distribution function (≈ 4.5 and ≈ 2.8 Å, respectively). Following Refs. 30 and 34, we select $b/a = 1.72$, $c/a = 3$, and $U_R/U_A = 3.5$. This choice of parameters produces a phase diagram with several water-like features. It includes two critical points, one corresponding to the first-order liquid-gas transition and the other to a first-order liquid-liquid transition at low temperatures, and a wide region of density anomaly bounded by the locus of temperatures of maximum density. The role of the attractive potential, $b \leq r \leq c$, is simply to allow fluid-fluid transitions to occur. Water-like thermodynamic, dynamic, and structural anomalies occur

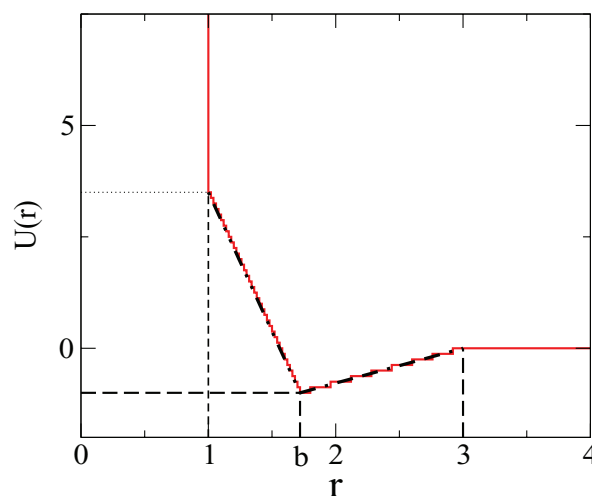


FIG. 1. Water is modelled by the spherically symmetric “two length scale” (a and b) Jagla ramp potential.²¹ The continuous form of the potential (black line) is used in umbrella sampling to calculate the potential of mean force between a pair of hard spheres. The discretized form (red line) of the potential is used in event driven molecular dynamics. $a = 1$ is the diameter of a Jagla sphere.

even in the purely repulsive case ($U_A = 0$), and their appearance is governed by the ratio b/a .³⁶

To compare the PMF calculated using the umbrella sampling method via Monte Carlo simulations of the continuous potential, we also calculate the PMF using a methodology developed in the previous works, the discrete molecular dynamics (DMD) method.^{21,37–41} In order to use the DMD algorithm, we replace the repulsive and attractive ramps with discrete steps (40 and 8, respectively), as described in Ref. 30 (see Fig. 1).

We measure length in units of a , time in units of $a(m/U_A)^{1/2}$ (where m is the particle mass), the number density in units of a^{-3} , pressure in units of $U_A a^{-3}$, energy in units of U_A , and temperature in units of U_A/k_B . This realization of the Jagla model displays a liquid-gas critical point at $T_{c1} = 1.446$, $P_{c1} = 0.0417$, and $\rho_{c1} = 0.102$, and a liquid-liquid critical point at $T_{c2} = 0.375$, $P_{c2} = 0.243$, and $\rho_{c2} = 0.370$.³⁰

We model solute particles as hard spheres with a diameter d_0 . The hard sphere solutes interact with the Jagla solvent only through excluded volume repulsion, which occurs at a contact distance of $(a + d_0)/2$. Here, we consider $d_0 = a$ to be the hard core diameter of the solute. The dependence of the solubility on d_0 is an important question and will be the subject of future work.

Keeping the pressure of the solvent constant at $P = 0.1$, we study five state points $T = 2$, $\rho = 0.0788$, $T = 1.5$, $\rho = 0.1836$, $T = 1.2$, $\rho = 0.2228$, $T = 0.9$, $\rho = 0.2493$, and $T = 0.5$, $\rho = 0.2658$. The constant pressure line passes below the liquid-liquid critical point and above liquid-gas critical point. The system size is set at $N = 1000, 2000$, and the number of independent configurations analyzed is above 1200. Independent configurations are stored for each set of 50 000 MC sweeps, for further analysis.

The PMF between two solutes quantifies the net interaction between the solute particles as a result of both direct and solvent-mediated interactions. In general, we define the PMF

through the average distribution function $\langle p(\xi) \rangle$ subject to the constraint of fixing some coordinate ξ to a given value. In our case, the relevant coordinate is the distance between the solute particles. Thus, we write

$$\langle p(\xi) \rangle = \frac{\int d\mathbf{R} \delta(\xi(\mathbf{R}) - \xi) \exp(-U(\mathbf{R})/k_B T)}{\int d\mathbf{R} \exp(-U(\mathbf{R})/k_B T)}, \quad (1)$$

where \mathbf{R} represents the $3N$ dimensional configuration space coordinates of the system (for an N atomic system). With respect to a reference value ξ^* of the relevant coordinate, we can define the PMF $W(\xi)$ to be

$$W(\xi) \equiv W(\xi^*) - k_B T \ln \left[\frac{\langle p(\xi) \rangle}{\langle p(\xi^*) \rangle} \right]. \quad (2)$$

In calculating the PMF we have employed three methods: umbrella sampling, directly calculating the mean force, and calculating the distance-dependent excess chemical potential.

A. Umbrella sampling

Although the PMF can be evaluated using simulations that generate a distribution of the distances between pairs of solvent particles, the probability of finding two solutes at any given range of distances is prone to large statistical error. Thus, we first use the umbrella sampling method to evaluate the PMF. In the umbrella sampling method, we perform Monte Carlo simulations with a bias potential added to the bare interaction potential of the system. The bias potential is set so that it forces the solute particles to sample a desired range of distances. Thus, we add a harmonic potential $w_i(\xi) = \frac{1}{2} K (\xi - \xi_i)^2$, where ξ_i is the most probable value of ξ in umbrella sampling run i , and it generates a biased distribution function $p(\xi)^b$. It can be easily verified that the potential of mean force is obtained in terms of the biased distribution as⁴²

$$W_i(\xi) = W(\xi^*) - k_B T \ln \left[\frac{\langle p(\xi)^b \rangle}{\langle p(\xi^*) \rangle} \right] - w_i(\xi) + F_i, \quad (3)$$

where the unknown constant F_i is given by

$$\exp^{-F_i/k_B T} = \langle \exp^{-w_i(\xi)/k_B T} \rangle. \quad (4)$$

The ensemble averages indicated by $\langle \dots \rangle$ above are computed as usual by the average of the quantity of interest over a series of configurations obtained after each MC step; specifically, $\langle p(\xi)^b \rangle$ is the frequency of observing a configuration in which the distance between two solutes is equal to ξ .

By performing a series of umbrella sampling runs, we have estimates of the PMF W_i in different windows of ξ , each shifted with respect to the other by an unknown constant F_i [see Eq. (3) above], which is eliminated by requiring that the PMF estimated using the different bias potentials match for the same values of ξ . Using an appropriate value for the spring constant K (we choose $K = 9.0$), and setting the spacing between successive ξ_i such that the distributions $\langle p(\xi)^b \rangle$ have sufficient overlap with good statistics, the full PMF is generated by shifting the individual estimates with respect to each other so that they match in the ξ range of overlap. In practice, we use a nonlinear fit to the set of PMF estimates W_i , with

a different ξ independent constant term for each run i with a different bias potential w_i , the other fit parameters being the same for all cases.

B. Direct calculation of the mean force

In this method, we compute the PMF by first calculating the mean force $F(r)$ acting between two solute particles separated by a distance r using DMD simulations. Since the solutes have only hard sphere repulsion, the mean force arises from interactions with the solvent particles. We consider two solutes confined by an imposed square-well potential to a limited range of separating distances R ,

$$U_{\text{bond}}(R) = \begin{cases} \infty & R < d_1 \\ 0 & d_1 < R < d_2 \\ \infty & R > d_2 \end{cases}, \quad (5)$$

where $(d_1 + d_2)/2 = r$, the separation at which we wish to calculate $F(r)$ and $d_2 - d_1 = \Delta r = 0.1a$. To find $F(r)$, we compute the sum $\sum \Delta p_r / 2$ of changes of the radial component of the linear momentum for both solute particles due to collisions with all Jagla particles and divide it by the total simulation time, $F(r) = \frac{1}{\Delta t} \sum \Delta p_r$. The radial component is the projection of the momentum change of the first particle on the radius vector directed from the second particle to the first particle. In these simulations we first equilibrate the system at constant P and T to establish its equilibrium volume $V(T, P)$ and then perform a production run for constant V and T . The simulations are done for $N = 1000$ Jagla particles and two hard spheres for $t = 10^4$ time units. We compute the potential of mean force by integrating $F(r)$ from a sufficiently large cutoff $r_{\text{max}} = 5a$ to a given $r < r_{\text{max}}$,

$$W(r) = W(r_{\text{max}}) + \int_r^{r_{\text{max}}} F(r) dr, \quad (6)$$

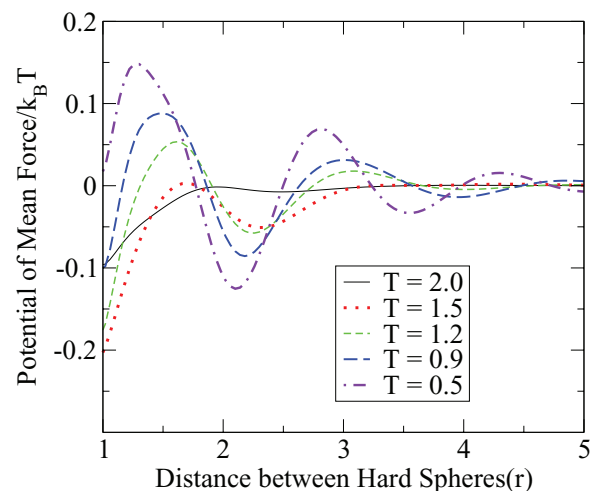


FIG. 2. The potential of mean force $W(r)$ (divided by $k_B T$) vs. distance between two hard spheres immersed in the Jagla solvent shown for five temperatures at pressure $P = 0.1$. The lines shown are fit lines obtained by umbrella sampling. The comparison of PMF calculated by different methods is shown in Fig. 3.

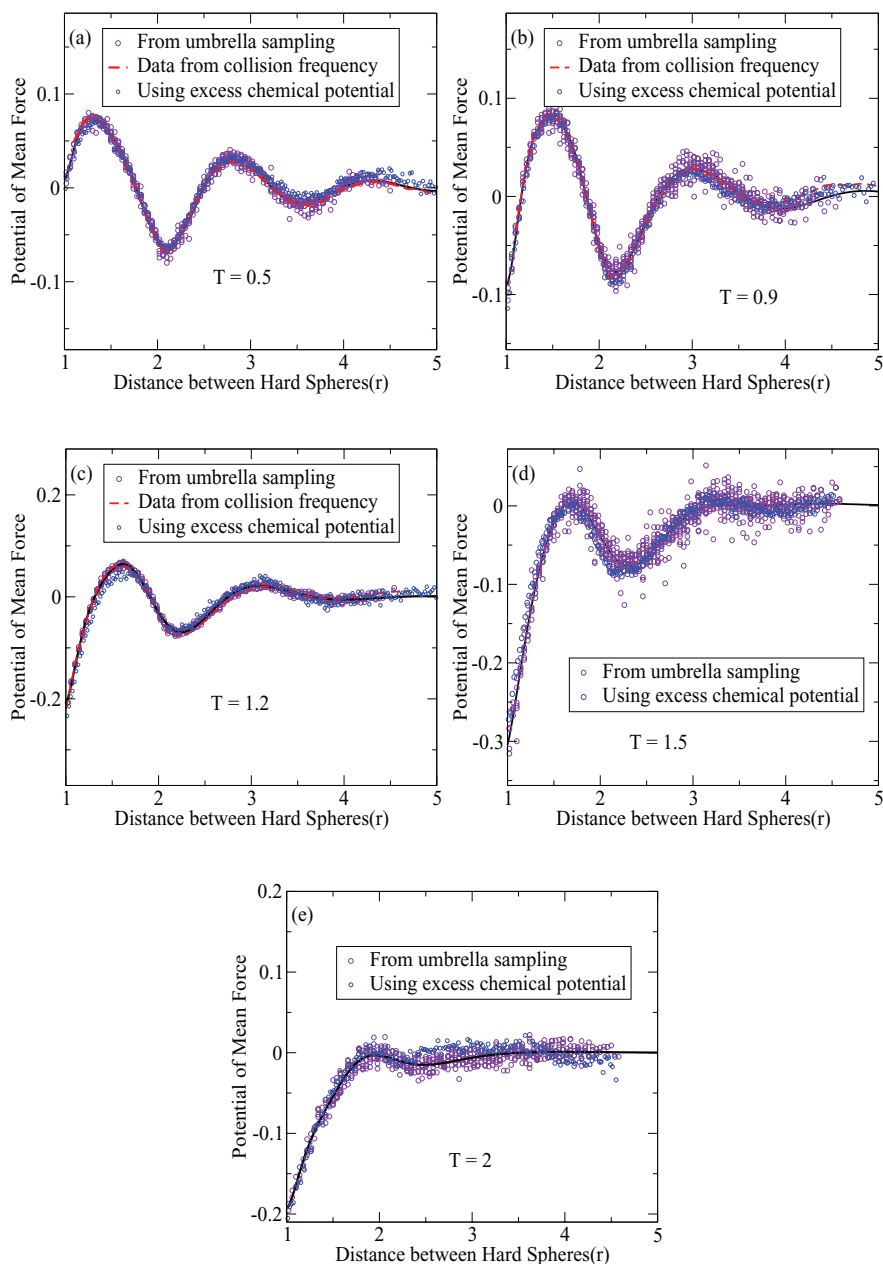


FIG. 3. Comparison of PMF obtained from three different methods, shown in a different panel for each temperature. The data shown by violet circles are from different umbrella sampling runs, after they have been shifted to yield the fit curve shown in Fig. 2 (also shown here). Thus, the scatter in the data points indicates the accuracy of the determination of PMF. The data points shown in blue squares are from the excess chemical potential (see Sec. II B). The PMF curves shown in red dashed lines are obtained using the collision frequency (see text). The results from the three methods agree well with each other.

where $W(r_{\max})$ is approximated as the logarithm of the solute-solute radial distribution function in the diluted solvent, $W(r_{\max}) = -k_B T \ln [g(r_{\max})]$.

C. Distance dependent excess chemical potential

The third approach we use to calculate the PMF is based on the excess chemical potential μ^{ex} of a solute, as a function of the distance from a second solute particle. In the limit of the distance between the two solutes $\xi \rightarrow \infty$, one obtains the bulk value of the excess chemical potential $\mu_{\text{bulk}}^{\text{ex}}$, whereas at finite distances the difference of $\mu^{\text{ex}}(\xi)$ and $\mu_{\text{bulk}}^{\text{ex}}$ yields the

potential of mean force.^{43,44} We generate equilibrium configurations using Monte Carlo *NVT* runs of a system of one solute in a sea of solvent molecules. The excess chemical potential of a second solute is calculated as a function of distance ξ from the first solute using a geometrical analysis⁴⁵ to find the void space available for the insertion of the second solute particle. In order to do so, we consider spherical shells at varying distances from the solute particle, and evaluate the volume fraction in each shell that is in the void, i.e., the volume fraction that is available for the insertion of the second solute particle. Then

$$\mu_s^{\text{ex}}(\xi) = -k_B T \ln(\langle v_0(\xi) \rangle), \quad (7)$$

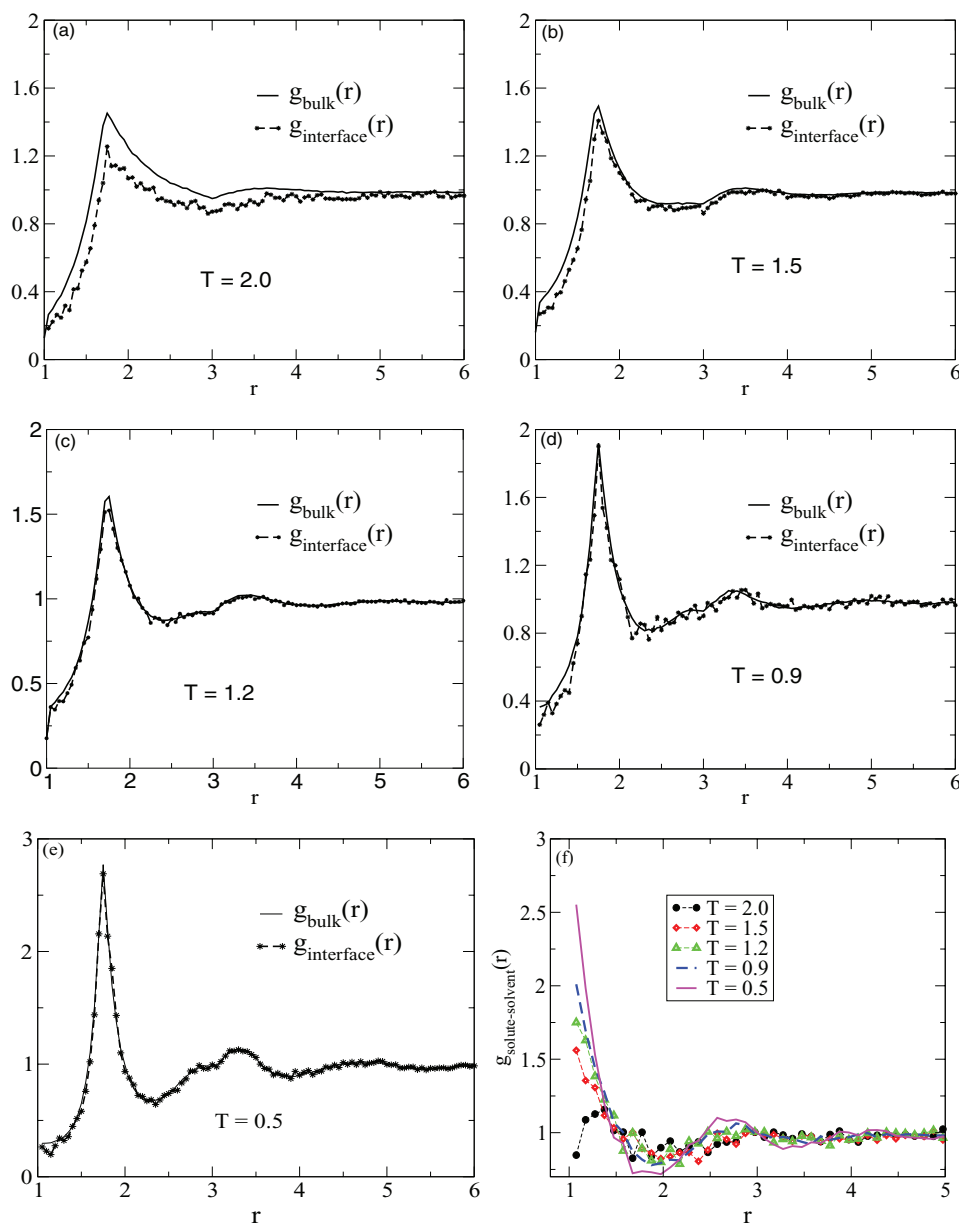


FIG. 4. (a)–(e) The pair correlation function $g(r)$ of the solvent, in the bulk (solid line) and near the hard sphere solute (symbols). The local structure is almost unaffected by the presence of the solute at low T whereas at high T , the interfacial solvent structure is perturbed. (f) Solvent-Solute pair correlation function, which is more strongly peaked at lower temperature.

$$W(\xi) = \mu_s^{\text{ex}}(\xi) - \mu_{\text{bulk}}^{\text{ex}}, \quad (8)$$

where $v_0(\xi)$ is the volume fraction for a given bin labeled by ξ that is in the void. Averaging is performed on the number of equilibrium configurations (typically 2500) to find out $\langle v_0(\xi) \rangle$. This method is the standard Widom insertion method for calculating the excess chemical potential⁴⁶ as it applies to hard particles. We use the algorithm of finding void space described in Ref. 45.

1. Cavity correlation function

As a related geometrical characterization of the solvent structure, we calculate the cavity correlation function $S_2(r)$,⁴⁷ which is the probability that two randomly chosen points separated by a distance r both lie in the void space, i.e., that it is

possible to insert the solute particle at either of the two locations without hard core overlaps with the solvent particles. As $r \rightarrow 0$, $S_2(r) \rightarrow \langle v_0 \rangle$ where $\langle v_0 \rangle$ is the volume fraction of the void space mentioned above. As $r \rightarrow \infty$, $S_2(r) \rightarrow \langle v_0 \rangle^2$.

III. RESULTS

The PMF $W(r)$ divided by $k_B T$ between hard sphere solutes at different temperatures obtained from umbrella sampling are shown in Fig. 2. The data shown are the fit lines to the PMF using the procedure described above. The results for the three different methods used are compared in Fig. 3, with a different panel for each temperature. The data shown for umbrella sampling are the individual data points from all the sampling runs, shifted in each case by the constant factor

explained above. These data thus provide an estimate of the error in our computation. The results from all three methods are in good agreement.

We begin by focusing on the first minimum of the PMF, which corresponds to a separation near d_0 between the two hard sphere solutes. The PMF at contact shows non-monotonic behavior with temperature, displaying a trend that is consistent with the solubility of the hydrophobic homopolymer presented in Ref. 30. The state point with $T = 1.5$, $\rho = 0.1836$ has the lowest PMF value at contact, and then increases upon both increasing and decreasing temperature. This corresponds to a “hydrophobic collapse” regime at intermediate temperatures, with a weakening of the effective interaction between solute particles upon both increasing and decreasing temperature. That weakening occurs when the temperature is lowered implies the possibility of cold denaturation of polymers composed of hard sphere monomers. We also observe, however, that the second minimum of the PMF gets progressively deeper as the temperature is lowered. This implies that, at low temperatures, it becomes thermodynamically favorable for solutes to organize at distances separated by a solvent particle.

To better understand this phenomenon, we calculate the pair correlation function between solvent particles in the bulk solvent (i.e., separated from the solute particles by at least $6d_0$), and those solvent particles that are geometric neighbors of the solutes (identified by a Voronoi construction). As seen in Fig. 4, at high temperatures the pair correlation function near the solute particles ($g_{\text{interface}}(r)$) is different from the bulk $g(r)$, indicating that the presence of the solute affects the solvent structure. As the temperature is lowered, this difference gradually diminishes and, at the lowest temperature, the interface and bulk pair correlation functions are indistinguishable. Thus, at the lowest temperatures, the insertion of the solute does not affect the solvent structure at all, a situation that can arise whenever the solvent structure provides favorable positions for the embedding of the solute particles. An inspection of the solvent-solute pair correlation function (Fig. 4) shows

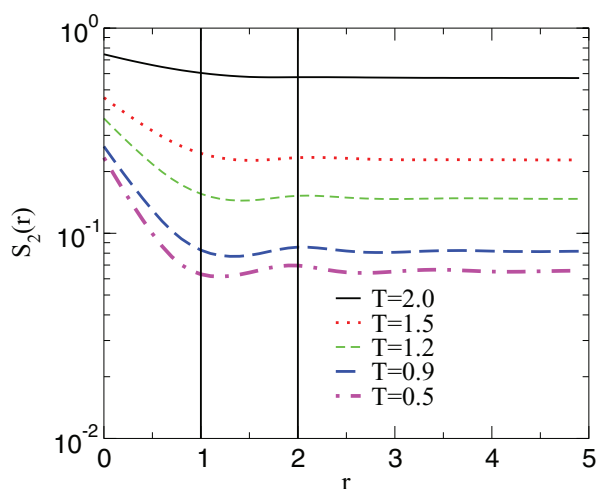


FIG. 5. The cavity correlation of Jagla fluid. The emergence of a peak at the solvent separated distance of $r = 2a$ at low temperatures implies that it becomes favorable for the solute spheres to be at solvent separated positions. Solute at such a separation will perturb the solvent structure the least.

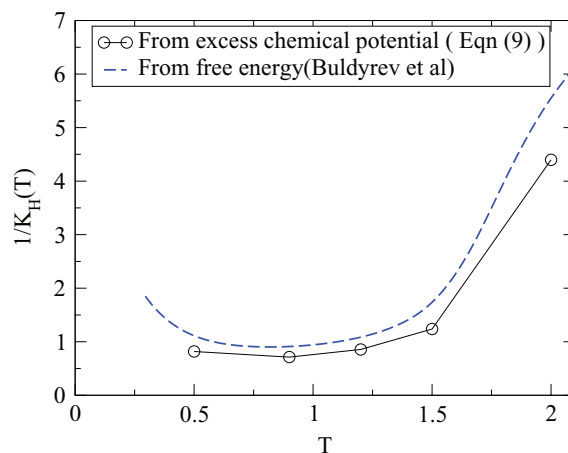


FIG. 6. Inverse of Henry constant $K_H(T)$ vs. temperature, whose minimum corresponds to a minimum of the solubility. The Henry constant, calculated directly from the excess chemical potential here, is compared with the estimate of Buldyrev *et al.*²⁰ near the location of minimum solubility.

that, indeed, this pair correlation becomes stronger at the contact position as the temperature is lowered.

To investigate further the ordering at low temperatures, we calculate the cavity correlation function in the pure solvent (see Fig. 5). This correlation function reveals the structure of the void space into which a solute particle may be inserted. Note that, as the temperature decreases, a peak in the cavity correlation function develops at a distance of $2a$ (which is equal to $d_0 + a$ for our choice of solvent and solute sizes). Thus, spatially correlated, solvent-separated locations exist in the solvent at which a pair of solute particles can be inserted with minimal perturbation of the solvent structure. We therefore conclude that the second minimum in the PMF arises from the structural ordering in the solvent at low temperatures, which makes it favorable for the solute particles to sit at solvent separated distances. Conversely, we conclude that the interpenetration of the solvent and solute particles at low temperatures is a possible mechanism for cold denaturation.

The solubility of hard spheres at low pressure can be well described using the Henry constant. The Henry constant $k_H(T)$ (Ref. 48) of the solute in the dilute mole fraction solution is defined as

$$K_H(T) \equiv k_B T \rho_\ell \exp\left(\frac{\mu_s^{\text{ex}}}{k_B T}\right), \quad (9)$$

where μ_s^{ex} is the excess chemical potential of the solute in the bulk, which we calculate directly by computing the void volume fraction, and ρ_ℓ is the number density of the solvent. The minimum solubility has a maximum value of $K_H(T)$, so the inverse of the Henry constant vs. T passes through a minimum shown in Fig. 6. This result is in good quantitative agreement with the results from previous work^{20,21} (also shown in Fig. 6) giving the temperature of minimum solubility near $T = 0.9$. A similar result using a one-dimensional lattice model was obtained in Ref. 49.

IV. CONCLUSION

We have calculated the PMF between hard sphere solutes immersed in a liquid displaying water-like properties and

defined by the Jagla model potential. We have calculated the PMF over a range of temperatures at constant pressure that spans a temperature range within which it was previously shown that a hard sphere homopolymer displays a collapse transition that is bracketed by regions in which one observes an analog of heat and cold denaturations in proteins. The PMF estimates obtained here using three different methods yield PMF values at contact that are consistent with an intermediate temperature regime in which the effective interaction at contact between hard sphere solutes is attractive, with the effective interaction at contact becoming unfavorable as the temperature is either increased or decreased. On the other hand, the effective interaction, quantified by the PMF, is seen as becoming progressively more attractive at a solvent-separated distance $2a$. By calculating the solvent pair correlation function near the solute and away from the solute, we have shown that the perturbation of solvent structure by the solute diminishes as the temperature decreases. We have calculated the cavity correlation function and demonstrated that a solvent-separated peak develops when the temperature is lowered. Taken together, these observations suggest a mechanism for cold denaturation that occurs because the solvent penetrates between hydrophobic solutes in configurations with favorable free energy. Our results thus suggest that cold denatured proteins are structured and that cold denaturation arises from strong solvent-solute interactions, rather than from entropic considerations as in heat denaturation.

ACKNOWLEDGMENTS

S.V.B. acknowledges the partial support of this research through the Dr. Bernard W. Gamson Computational Science Center at Yeshiva College. H.E.S. thanks the National Science Foundation (NSF) Chemistry Division (Grant Nos. CHE 0911389 and CHE 0908218) for support. S.S. and M.M. thank JNCASR and DST, India for computational resources. H.E.S., S.S., and M.M. thank the NSF Chemistry Division for support (Grant Nos. CHE-0404673, CHE 0911389, and CHE 0908218).

¹P. L. Privalov, *Crit. Rev. Biochem. Mol. Biol.* **25**, 281 (1990).

²K. A. Dill, *Biochemistry* **29**, 7133 (1990).

³P. L. Privalov, Y. V. Griko, S. Y. Venyaminov, and V. P. Kutysenko, *J. Mol. Biol.* **190**, 487 (1986).

⁴I. Nishii, M. Kataoka, F. Tokunaga, and Y. Goto, *Biochemistry* **33**, 4903 (1994).

⁵V. R. Agashe and J. B. Udgaonkar, *Biochemistry* **34**, 3286 (1995).

⁶J. Zipp and W. Kauzmann, *Biochemistry* **12**, 4217 (1973).

⁷J. Zhang, X. Peng, A. Jonas, and J. Jonas, *Biochemistry* **34**, 8631 (1995).

⁸G. Hummer, S. Garde, A. E. García, M. E. Paulaitis, and L. R. Pratt, *Proc. Natl. Acad. Sci. U.S.A.* **95**, 1552 (1998).

⁹S. Kunugi and N. Tanaka, *Biochem. Biophys. Acta* **1595**, 329 (2002).

¹⁰M. I. Marques, J. M. Borreguero, H. E. Stanley, and N. V. Dokholyan, *Phys. Rev. Lett.* **91**, 138103 (2003).

¹¹W. Kauzmann, *Adv. Protein Chem.* **14**, 1 (1959).

¹²F. H. Stillinger, *J. Solution Chem.* **1**, 141 (1973).

¹³L. R. Pratt and D. Chandler, *J. Chem. Phys.* **67**, 3683 (1977).

¹⁴G. Hummer and S. Garde, *Phys. Rev. Lett.* **80**, 4193 (1998).

¹⁵S. Garde, G. Hummer, A. E. García, L. R. Pratt, and M. E. Paulaitis, *Phys. Rev. E* **53**, R4310 (1996).

¹⁶R. Godawat, S. N. Jamadagni, and S. Garde, *Proc. Natl. Acad. Sci. U.S.A.* **106**, 15119 (2009).

¹⁷S. Sarupriya and S. Garde, *Phys. Rev. Lett.* **103**, 037803 (2009).

¹⁸G. Goel, M. V. Athawale, S. Garde, and T. M. Truskett, *J. Phys. Chem.* **112**, 13193 (2008).

¹⁹H. S. Ashbaugh, T. M. Truskett, and P. G. Debenedetti, *J. Chem. Phys.* **116**, 2907 (2002).

²⁰S. V. Buldyrev, P. Kumar, P. G. Debenedetti, P. J. Rossky, and H. E. Stanley, *Proc. Natl. Acad. Sci. U.S.A.* **104**, 20177 (2007).

²¹S. V. Buldyrev, P. Kumar, S. Sastry, H. E. Stanley, and S. Weiner, *J. Phys.: Condens. Matter* **22**, 284109 (2010).

²²B. A. Patel, P. G. Debenedetti, F. H. Stillinger, and P. J. Rossky, *Biophys. J.* **93**, 4116 (2007).

²³B. A. Patel, P. G. Debenedetti, and F. H. Stillinger, *J. Phys. Chem. A* **111**, 12651 (2007).

²⁴Y. S. Djikaev and E. Ruckenstein, *J. Chem. Phys.* **131**, 045105 (2009).

²⁵F. Franks, *Water: A Matrix for Life*, 2nd ed. (Royal Society of Chemistry, Cambridge, 2000).

²⁶D. Eisenberg and W. Kauzmann, *The Structure and Properties of Water* (Oxford University Press, New York, 1969).

²⁷P. G. Debenedetti, *J. Phys.: Condens. Matter* **15**, R1669 (2003).

²⁸P. G. Debenedetti and H. E. Stanley, *Phys. Today* **56**(6), 40 (2003).

²⁹E. A. Jagla, *Phys. Rev. E* **58**, 1478 (1998).

³⁰L. Xu, S. V. Buldyrev, C. A. Angell, and H. E. Stanley, *Phys. Rev. E* **74**, 031108 (2006).

³¹P. J. Flory, R. A. Orwoll, and A. Virj, *J. Am. Chem. Soc.* **86**, 3507 (1964).

³²A. Y. Grosberg and A. R. Khokhlov, *Giant Molecules* (Academic, London, 1997).

³³M. Rubinstein and R. H. Colby, *Polymer Physics* (Oxford University Press, New York, 2003).

³⁴L. Xu, P. Kumar, S. V. Buldyrev, S.-H. Chen, P. H. Poole, F. Sciortino, and H. E. Stanley, *Proc. Natl. Acad. Sci. U.S.A.* **102**, 16558 (2005).

³⁵Z. Yan, S. V. Buldyrev, N. Giovambattista, P. G. Debenedetti, and H. E. Stanley, *Phys. Rev. E* **73**, 051204 (2006).

³⁶Z. Yan, S. V. Buldyrev, N. Giovambattista, and H. E. Stanley, *Phys. Rev. Lett.* **95**, 130604 (2005).

³⁷D. Frenkel and B. Smit, *Understanding Molecular Simulation: From Algorithms to Applications* (Academic, San Diego, 1996).

³⁸D. C. Rapaport, *The Art of Molecular Dynamics Simulation* (Cambridge University Press, Cambridge, England, 1997).

³⁹B. J. Alder and T. E. Wainwright, *J. Chem. Phys.* **31**, 459 (1959).

⁴⁰D. C. Rapaport, *J. Phys. A* **11**, L213 (1978).

⁴¹S. V. Buldyrev, "Application of discrete molecular dynamics to protein folding and aggregation," in *Aspects of Physical Biology. Series: Lecture Notes in Physics*, edited by G. Franzese and M. Rubi (Springer-Verlag, Berlin/Heidelberg, 2008), pp. 97–132.

⁴²B. Roux, *Comput. Phys. Commun.* **91**, 275 (1995).

⁴³J. Forsmann and B. Jönsson, *J. Chem. Phys.* **101**, 5116 (1994).

⁴⁴S. Shimizu and H. S. Chan, *J. Chem. Phys.* **113**, 4683 (2000).

⁴⁵S. Sastry, D. S. Corti, P. G. Debenedetti, and F. H. Stillinger, *Phys. Rev. E* **56**, 5524 (1997).

⁴⁶B. Widom, *J. Chem. Phys.* **39**, 2808 (1963).

⁴⁷J. M. Haile, C. Massobrio, and S. Torquato, *J. Chem. Phys.* **83**, 4075 (1985).

⁴⁸J. R. Errington, G. C. Boulougouris, I. G. Economou, A. Z. Panagiotopoulos, and D. N. Theodorou, *J. Phys. Chem. B* **102**, 8865 (1998).

⁴⁹K. Koga, *J. Chem. Phys.* **121**, 7304 (2004).